

THE CLUSTERING OF MASSIVE HALOS

ANDREW R. WETZEL,^{1,2} J. D. COHN,^{1,3} MARTIN WHITE,^{1,4} DANIEL E. HOLZ,^{2,5} AND MICHAEL S. WARREN²
Received 2006 June 28; accepted 2006 October 24

ABSTRACT

The clustering properties of dark matter halos are a firm prediction of modern theories of structure formation. We use two large-volume, high-resolution N -body simulations to study how the correlation function of massive dark matter halos depends on their mass, assembly history, and recent merger activity. We find that halos with the lowest concentrations are currently more clustered than those of higher concentration, the size of the effect increasing with halo mass; this agrees with trends found in studies of lower mass halos. The clustering dependence on other characterizations of the full mass accretion history appears weaker than the effect with concentration. Using the integrated correlation function, marked correlation functions, and a power-law fit to the correlation function, we find evidence that halos that have recently undergone a major merger or a large mass gain have slightly enhanced clustering relative to a randomly chosen population with the same mass distribution.

Subject headings: cosmology: theory — dark matter — galaxies: clusters: general — methods: numerical

Online material: color figures

1. INTRODUCTION

The observed universe contains order on all scales we can probe. It is generally believed that the largest structures arose via the amplification of primordial (quantum) fluctuations during a period of accelerated expansion, processed by the subsequent 13 Gyr of gravitational instability. The pattern of clustering of objects on large scales is a calculable prediction of cosmological models and thus comprises one of the fundamental cosmological statistics.

Within modern theories of structure formation, the clustering of rare, massive dark matter halos is enhanced relative to that of the general mass distribution (Kaiser 1984; Efstathiou et al. 1988; Cole & Kaiser 1989; Mo & White 1996; Sheth & Tormen 1999), an effect known as bias. The more massive the halo, the larger the bias. As a result, the mass of halos hosting a given population of objects is sometimes inferred by measuring their degree of clustering, allowing a statistical route to the notoriously difficult problem of measuring masses of cosmological objects (e.g., Cooray & Sheth 2002).

Since halos of a given mass can differ in their formation history and large-scale environment,⁶ a natural question arises: do these details affect halo clustering? In currently viable scenarios for structure formation, objects grow either by accretion of smaller units or by major mergers with comparable-sized objects. The formation history of a halo can thus be characterized by its mass accumulation over time, such as when it reached half of its mass, had a mass jump in a short time, or last underwent a (major) merger.

Theoretically, the simplest descriptions of halo growth and clustering (Bond et al. 1991; Bower 1991; Lacey & Cole 1993, 1994; Kitayama & Suto 1996a, 1996b) do not give a dependence on halo formation history (White 1996; Sheth & Tormen 2004; Furlanetto & Kamionkowski 2006; Harker et al. 2006). To reprise these arguments, pick a random point in the universe and

imagine filtering the density field around it on a sequence of successively smaller scales. The enclosed density executes a random walk, which in the usual prescription is taken to be uncorrelated from scale to scale. The formation of a halo of a given mass corresponds to the path passing a certain critical value of the density, δ_c , at a given scale. The bias of the halo is the “past” of its random walk and its history the “future” of the walk. All halos of the same mass at that time correspond to random walks crossing the same point and thus have the same bias. (Note that the derivation, using sharp k -space filtering, does not match the way the prescription is usually applied, and this has been suggested by some of the above authors as a way to obtain history dependence. Introducing an environmental dependence through, e.g., elliptical collapse will also give a history dependence.)

The lack of dependence on halo history in the simplest descriptions does not close the discussion theoretically or otherwise. While these analytic methods work much better than might be expected given their starting assumptions, the Press-Schechter-based approaches still suffer many known difficulties (e.g., Sheth & Pitman 1997; Benson et al. 2005). Other analytical ways of estimating the clustering of mergers have been explored. For example, Furlanetto & Kamionkowski (2006) defined a merger kernel (not calculable from first principles) and assumed that all peaks within a certain volume eventually merged. Such an *Ansatz* implies that recently merged halos are more clustered for $M > M_*$ and less clustered for $M < M_*$, with some dependence on predecessor mass ratios and redshifts. [Here $M_*(z)$ is the mass at which $\sigma(M)$, the variance of the linear power spectrum smoothed on scale M , equals the threshold for linear density collapse $\delta_c(z)$; see, e.g., Peacock 1999.] Using close pairs as a proxy for recently merged halos, they found a similar enhancement of clustering for $M > M_*$ and reduction for $M < M_*$ in several (analytic) clustering models. To foreshadow our results, the signals we see are consistent with this trend.

Simple analytic models cannot be expected to capture all of the complexities of halo formation in hierarchical models, and full numerical simulations are required to validate and calibrate the fits. Fortunately, numerical simulations are now able to produce samples with sufficient statistics to test for the dependence of clustering on formation history. Early work by Lemson & Kauffmann (1999) showed that the properties of dark matter halos, in particular

¹ Department of Astronomy, University of California, Berkeley, CA.

² Theoretical Division, Los Alamos National Laboratory, Los Alamos, NM.

³ Space Sciences Laboratory, University of California, Berkeley, CA.

⁴ Department of Physics, University of California, Berkeley, CA.

⁵ Department of Astronomy and Astrophysics, University of Chicago, Chicago, IL.

⁶ The large-scale environment of a halo refers to the density, smoothed on some scale larger than the halos, e.g., $5\text{--}10 h^{-1}$ Mpc.

formation times, are little affected by their large-scale environment if the entire population of objects is averaged over. They interpreted this as evidence against formation history and environment affecting clustering. As emphasized by Sheth & Tormen (2004), however, this finding, plus the well-known fact that the typical mass of halos depends on local density, implies that the clustering of halos of the same mass must also depend on formation time. Using a marked correlation function, Sheth & Tormen (2004) found that close pairs tend to have earlier formation times than more distant pairs, work that was extended and confirmed by Harker et al. (2006). Gao et al. (2005) found that later forming, low-mass halos are less clustered than typical halos of the same mass at the present; a possible explanation of this result was given by Wang et al. (2006). Wechsler et al. (2006) found a similar dependence on halo formation time, showing that the trend reversed for more massive halos and that the clustering depended on halo concentration. However, in order to probe to higher masses, these authors assumed that the mass dependence was purely a function of the mass in units of the nonlinear mass and then used earlier outputs to probe to higher values of this ratio. It should be noted that scaling quantities by M/M_* gives a direct equality only if clustering is self-similar. Since $P(k)$ is not a power law and $\Omega_{\text{mat}} \neq 1$, a check of this approximation, as is done here, is crucial.

These formation time dependencies are based on (usually smooth) fits to the accretion history of the halo. However, halo assembly histories are often punctuated by large jumps from major mergers that have dramatic effects on the halos. Major mergers can be associated with a wide variety of phenomena, ranging from quasar activity (Kauffmann & Haehnelt 2000) and starbursts in galaxies (Mihos & Hernquist 1996) to radio halos and relics in galaxy clusters (for phenomena associated with galaxy cluster mergers see, e.g., Sarazin 2005⁷). Major mergers of galaxy clusters are the most energetic events in the universe. It follows that major merger phenomena can either provide signals of interest or cause noise in selection functions that depend on a merger-affected observable. If recently merged halos cluster differently from the general population (merger bias), and this is unaccounted for, conclusions drawn about halos on the basis of their clustering would be suspect. The question of whether such merger bias exists remains unresolved, as previous work to identify a merger bias through N -body simulations and analytic methods yields mixed results (Gottlöber et al. 2002; Percival et al. 2003; Scannapieco & Thacker 2003; Furlanetto & Kamionkowski 2006).

In this paper we consider the clustering of the most massive dark matter halos, measured from two large-volume ($1.1 h^{-1} \text{ Gpc}$)³ N -body simulations described in § 2. We concentrate on massive halos, as most previous simulations did not have the volume to effectively probe this end of the mass function, and furthermore, for the largest mass halos the correspondence between theory and observation is particularly clean. We first examine the long-term growth history of halos, calculating the “assembly bias” as a function of growth history in § 4, extending previous results mentioned above to higher masses. We then look to short-term history effects (i.e., events), measuring the “merger bias” as a function of recent major merger activity or large mass gain in § 5, where we find a weak, but statistically significant, signal for both cases. We conclude in § 6.

2. SIMULATIONS

To investigate the effects of formation history on clustering statistics, we use two high-resolution N -body simulations performed

with independent codes: the HOT code (Warren & Salmon 1993) and the TreePM code (White 2002). Both simulations evolved randomly generated, Gaussian initial conditions for 1024^3 particles of mass $10^{11} h^{-1} M_{\odot}$ from $z = 34$ to the present, using the same Λ CDM cosmology ($\Omega_M = 0.3 = 1 - \Omega_{\Lambda}$, $\Omega_B = 0.046$, $h = 0.7$, $n = 1$, and $\sigma_8 = 0.9$) in a periodic, cubical box of side $1.1 h^{-1} \text{ Gpc}$. For the HOT simulation a Plummer law with softening $35 h^{-1} \text{ kpc}$ (comoving) was used. The TreePM code used a spline softened force with the same Plummer equivalent softening. The TreePM data were dumped in steps of light crossings of $136 h^{-1} \text{ Mpc}$ (comoving), producing 30 outputs from $z \approx 3$ to $z = 0$. The HOT data were dumped from $z \approx 1$ (look-back time of $5.3 h^{-1} \text{ Gyr}$) to $z = 0$ in intervals of $0.7 h^{-1} \text{ Gyr}$, with the last interval at $z = 0$ reduced to $0.4 h^{-1} \text{ Gyr}$. The outputs before $z \approx 1$ had so few high-mass halos that the statistics were not useful for the merger event calculations. For comparisons of how using light crossings versus fixed time steps in Gyr changes merger ratios, see Cohn & White (2005). The TreePM simulations were used for the assembly histories and the HOT simulations for the merger bias calculations, although the results from the two simulations were consistent so either could have been used in principle.

For each output we generate two catalogs of halos via the friends-of-friends (FoF) algorithm (Davis et al. 1985), using linking lengths $b = 0.2$ and 0.15 in units of the mean interparticle spacing. These groups correspond roughly to all particles above a density threshold $3/(2\pi b^3)$; thus, both linking lengths enclose primarily virialized material. Henceforth halo masses are quoted as the sum of the particle masses within FoF halos; thus, a given halo’s $b = 0.15$ mass will be smaller than its $b = 0.2$ mass (for more discussion see White 2001). We consider halos with mass $M > 5 \times 10^{13} h^{-1} M_{\odot}$ (more than 500 particles); at $z = 0$ there are approximately 96,000 such halos in each box for the $b = 0.15$ catalog and 120,000 for the $b = 0.2$ catalog. The mass functions and merger statistics from the two simulations are consistent within Poisson scatter.

Given a child-parent relationship between halos at neighboring output times, construction of the merger tree is straightforward since we are tracking massive halos rather than, e.g., subhalos. Progenitors are defined as those halos at an earlier time that contributed at least half of their mass to a later (child) halo. Of the approximately 10^5 halos at $z = 0$ we find only 14 for which our simple method fails. In these cases a “fly-by” collision of two halos gives rise to a halo at $z = 0$ with no apparent progenitors. Excluding these halos does not change our results. For the TreePM run, we use all 30 outputs to construct the merger tree, which stored all of the halo information (mass, velocity dispersion, position, etc.) for each halo at each output. Each node of the tree pointed to a linked list of its progenitors at the earlier time, enabling a traversal of the tree to find mass accretion histories and mergers. The HOT run produced outputs for each time interval of child and parent halos.

3. MEASURING CLUSTERING

A basic measure of clustering is the two-point function, which in configuration space is the correlation function, $\xi(r)$. To compute $\xi(r)$, we use the method of Landy & Szalay (1993):

$$\xi(r) = \frac{\langle DD \rangle - 2\langle DR \rangle + \langle RR \rangle}{\langle RR \rangle}, \quad (1)$$

where D and R are data and random catalogs, respectively, and the angle brackets refer to counts within a shell of small width having radius r . In computing $\langle DR \rangle$ and $\langle RR \rangle$ we use 10 times as

⁷ Available at <http://www.aoc.nrao.edu/events/xraydio>.

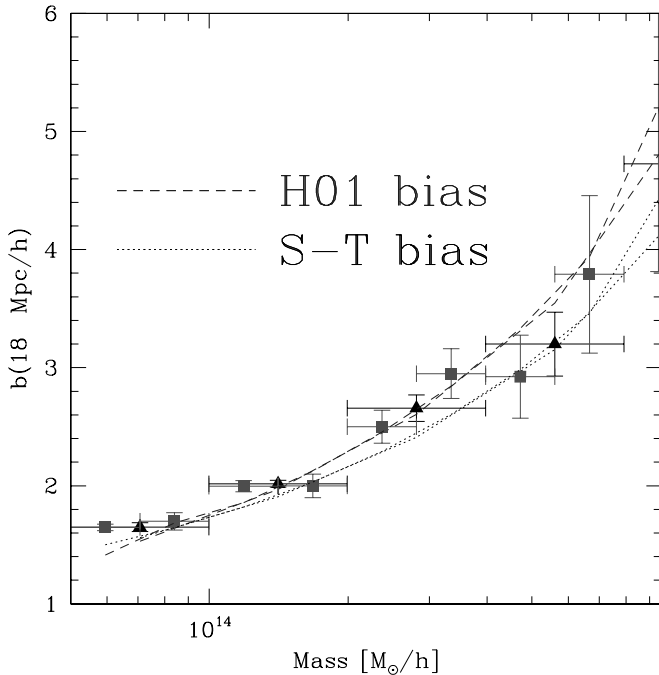


FIG. 1.—Bias $b(r) = [\xi(r)/\xi_{\text{dm}}(r)]^{1/2}$ at $r = 18 h^{-1}$ Mpc for two different binnings in mass. The horizontal error bars on each point show the range of masses used. The bias was approximately scale invariant in this mass regime from 15 to $30 h^{-1}$ Mpc. We show two fits to $b(M)$ proposed in the literature: that of Hamana et al. (2001) (dashed line) and that of Sheth & Tormen (1999) (dotted line), each plotted for both mass binnings. [See the electronic edition of the *Journal* for a color version of this figure.]

many random as data points. To compute errors, we divide the simulation volume into eight octants and compute $\xi(r)$ within each octant. Since we probe scales much smaller than the octants, we treat them as uncorrelated volumes, and we quote the mean $\xi(r)$ and error on the mean under this assumption. These errors tend to be ~ 1.4 – 2 times larger than the more approximate $(N_{\text{pair}})^{1/2}$ error estimates used in some previous work.

Our goal is to test the dependence of the clustering of objects associated with some history-dependent property. A relevant quantity for comparison is the (mass dependent) bias of the halos relative to the underlying dark matter, which we define as

$$\xi(r) = b^2 \xi_{\text{dm}}(r). \quad (2)$$

Analytically, the large-scale bias is related to a derivative of the halo mass function (Efstathiou et al. 1988; Cole & Kaiser 1989; Mo & White 1996; Sheth & Tormen 1999). For the Sheth-Tormen form of the mass function one finds

$$b_{\text{ST}}(M_{180\rho_b}) = 1 + \frac{\nu'^2 - 1}{\delta_c} + \frac{0.6}{\delta_c(1 + \nu'^{0.6})}, \quad (3)$$

where $\nu' = 0.841 \delta_c / \sigma(M_{180\rho_b})$ and $\delta_c = 1.686$. This has been improved on using the Hubble volume simulations (Colberg et al. 2000; Hamana et al. 2001); see also Seljak & Warren (2004) for discussion of the bias defined through $P(k)$ on similar scales. Hamana et al. (2001) used FoF halos with $b = 0.164$ and found

$$b(M, R, z) = b_{\text{ST}}(M_{108}, z) \times [1.0 + b_{\text{ST}}(M_{108}, z) \sigma_R(R, z)]^{0.15}. \quad (4)$$

The subscripts on the mass M indicate which overdensity threshold is being used to define the halo mass. We took $M = 0.93M_{108}$

and $M = 1.07M_{180b}$, calculating the conversion using the profile of Navarro et al. (1997) assuming a concentration $c = 5$. The change in conversion factor was less than a percent for the range of concentrations of interest. See White (2001) for more details, discussion, and definitions.

We show the bias $b = [\xi(r)/\xi_{\text{dm}}(r)]^{1/2}$ at $r = 18 h^{-1}$ Mpc as a function of mass in Figure 1. The bias for halos with $M > 5 \times 10^{13} h^{-1} M_{\odot}$ changed less than 5% on scales $r \geq 15 h^{-1}$ Mpc. We include the two bias fits given above for $r = 18 h^{-1}$ Mpc at $z = 0$. The Hamana et al. (2001) fit was derived from a larger simulation volume; Figure 1 is included to illustrate the mass dependence of the global bias, to provide a comparison context for the sizes of the additional biases of concern in this paper. We now turn to estimates of bias effects due to the history of the halos.

4. ASSEMBLY BIAS

We begin by considering parameterizations of the formation history of halos that emphasize the global properties, i.e., those related to the halo mass growth over a long period of time. We consider three parameterizations of halo histories that have previously been used with lower mass halos: c , $a_{1/2}$, and a_f (Wechsler et al. 2006; Gao et al. 2005; Sheth & Tormen 2004). Using these parameterizations, Sheth & Tormen (2004), Harker et al. (2006), Gao et al. (2005), Wechsler et al. (2006), and Croton et al. (2006) have shown that the clustering of halos of fixed mass is correlated with “formation time,” a result that has come to be termed assembly bias. The effect is strongest for smaller halos, and this has been the focus of earlier work. For the extremely massive halos that we consider, halo identification is simpler, as none of our halos are subhalos. However, since massive halos are rarer, the statistics are poor even for a simulation volume as large as ours.

The concentration, c , is a parameter in an NFW fit to a halo density profile (Navarro et al. 1997).⁸ We perform a least-squares fit of the NFW functional form to the radial mass distribution of all of the particles in the FoF group, allowing c and M_{200} to vary simultaneously. This is in order to be similar to the procedure of Bullock et al. (2001) to allow ready comparison. The concentration is expected to correlate with the time by which most of the halo formed (earlier forming halos are more concentrated; see Navarro et al. 1996; Wechsler et al. 2002; Gao et al. 2004). There is also a weak dependence of concentration on halo mass. We have tried to minimize this effect by dividing out the average concentration for each mass (calculated from the data) to get a “reduced” concentration, which is essentially uncorrelated with mass (correlation is less than 0.2%).

The second parameter encapsulating the formation history is $a_{1/2}$, the scale factor at which a halo accumulates half of its final mass. We find $a_{1/2}$ by linearly interpolating between the two bracketing times. Analytic properties of this definition have been studied in Sheth & Tormen (2004), and $a_{1/2}$ is often used as a proxy for formation epoch. The third parameter, a_f , the formation scale factor, is also a formation time proxy. It is defined through a fit to the halo mass accretion history (Wechsler et al. 2002):⁹

$$M(z) = M_0 \exp(-2a_f z), \quad (5)$$

where M_0 is the mass of the halo at $z = 0$. We calculate this from the history by doing a least-squares fit of $\ln(M_i/M_0)$ against z_i for all of the z_i steps. Although this form does not fit the mass

⁸ We follow NFW and take $c = r_{200}/r_s$; note that Wechsler et al. (2006) use $c_{\text{vir}} = r_{\text{vir}}/r_s$, where $r_{\text{vir}} \simeq r_{100}$ for our cosmology. At $z = 0$, $c_{\text{vir}} \simeq 1.25c$.

⁹ Miller et al. (2006) present an analytic justification for this form based on extended Press-Schechter theory.

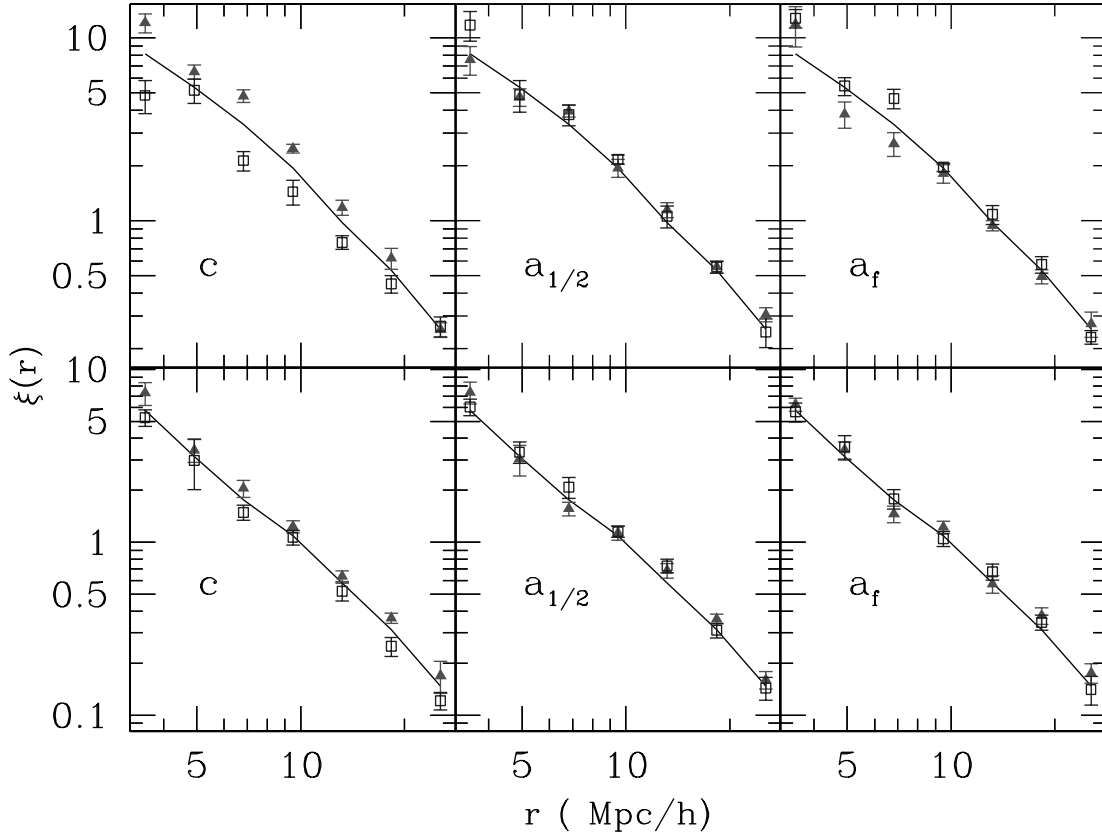


FIG. 2.—Correlation function of the lowest (*filled triangles*) and highest (*open squares*) quartiles of (reduced) concentration, c (*left*), half mass scale factor, $a_{1/2}$ (*middle*), and formation scale factor, a_f (*right*). The solid line is $\xi(r)$ for the full halo sample. *Top panels*: $10^{14} h^{-1} M_{\odot} \leq M \leq 3 \times 10^{14} h^{-1} M_{\odot}$ (31,551 halos). *Bottom panels*: $5 \times 10^{13} h^{-1} M_{\odot} \leq M \leq 8 \times 10^{13} h^{-1} M_{\odot}$ (43,638 halos). A clear signal is seen for concentration and formation scale factor for the more massive halos. [See the electronic edition of the *Journal* for a color version of this figure.]

accretion history of massive halos particularly well due to their frequent mergers, the fit is well defined and, as shown below, a_f nonetheless appears to be correlated with clustering.

The correlations¹⁰ for many of the above parameters were presented in Cohn & White (2005). Some of these correlations have been compared in different combinations in Wechsler et al. (2002, 2006), Zhao et al. (2003a, 2003b), and Croton et al. (2006). Except for Zhao et al. (2003a, 2003b), these were for galaxy-scale halos rather than galaxy cluster-scale halos. The formation histories for low-mass halos tend to be smoother and better fitted to the form of Wechsler et al. (2002) since they undergo fewer mergers than high-mass halos at late times. Wechsler and Zhao give a formula for the concentration in terms of the formation time of Wechsler et al. (2002); our correlation coefficient is characterizing the scatter around any such correlation. For the current sample the strongest correlation (0.69) is between the formation redshift, $z_f = 1/a_f - 1$, and the half-mass redshift, $z_{1/2} = 1/a_{1/2} - 1$, consistent with the 0.70 found by Cohn & White (2005) with a sample about $\frac{1}{7}$ the size. The formation redshift, z_f , and reduced concentration have a correlation of 0.53. The full concentration and $z_{1/2}$ (z_f) have a correlation of 0.56 (0.54). These correlations increase as the lower mass limit is decreased from 10^{14} to $5 \times 10^{13} h^{-1} M_{\odot}$.

To highlight any effects of assembly bias, we take the highest and lowest quartiles of the distribution of each of these three parameterization values and compare the resulting $\xi(r)$ to that of the full sample (similar to Wechsler et al. 2006). We show examples for $10^{14} h^{-1} M_{\odot} < M < 3 \times 10^{14} h^{-1} M_{\odot}$ and $5 \times$

$10^{13} h^{-1} M_{\odot} < M < 8 \times 10^{13} h^{-1} M_{\odot}$ in Figure 2. For the higher mass halos we see a strong dependence of clustering on concentration. We see a similar, but noticeably smaller, dependence on a_f , indicating that more recently formed objects cluster more strongly. As all of the objects we consider have $M > M_*$, our results are in line with the expectation of Wechsler et al. (2006) and the theoretical model of Furlanetto & Kamionkowski (2006). Specifically, this confirms the result found by Wechsler et al. (2006) at $z = 0$, without needing to make the approximation that $b(c, M, z) = b(c, M/M_*)$.

The ratio of their correlation function at their top c quartile to the total sample for halos $\sim 10M_*$ was ~ 1.25 . This is larger than our ratio, which does not reach 1.2 for any of the radii considered in Figure 2, although it is well within our (and their) errors. This is mirrored for the lowest c quartile where our effect is similarly reduced but within the errors. We are using reduced concentration, while they divide each halo's concentration by the average concentration in its mass bin, \bar{c}_{vir} . For the lower mass sample a much weaker trend is seen (e.g., the ratios for the quartiles when selected on concentration barely reach 10%), agreeing with the expectation that the signal decreases as $M \rightarrow M_*$. At fixed mass, the trend of b with c is consistent with the fit of Wechsler et al. (2006), but the trend is so weak relative to the noise that the result is of marginal significance.

Gao et al. (2005) and Harker et al. (2006) found bias for $M > M_*$ based on $z_{1/2}$, where both the lowest and highest quartiles of $z_{1/2}$ tended to be more clustered than the full sample. We see a hint of this as well, but the fluctuations are large. Croton et al. (2006) also found more dependence of clustering on $z_{1/2}$ (their formation time) than on concentration, once luminosity-dependent bias was

¹⁰ Defined as $\langle (ab) \rangle - \langle a \rangle \langle b \rangle / [(\langle a^2 \rangle - \langle a \rangle^2)(\langle b^2 \rangle - \langle b \rangle^2)]^{1/2}$; see, e.g., Lupton (1993).

taken out. Note that their luminosity dependence might include some of the history measured by concentration or $z_{1/2}$ and their focus was on galaxies populating the halos rather than the halos themselves.

Note also that even though z_f and $z_{1/2}$ are correlated, the correlation is not strong enough so that bias in one implies bias in the other. The overlap of the upper and lower quartiles for these quantities for $M > 10^{14} h^{-1} M_\odot$ is 62% and 54%, respectively. As the rest of the clusters differ, the overall biases can be quite different, as seen in Figure 2.

Another formation time-related quantity, the redshift of last mass jump by 20% or more in a time step corresponding to the light crossing time of $136 h^{-1}$ Mpc comoving, had correlations with $z_{1/2}$ (0.70), z_f (0.61), and c (0.40). We found a small sign of bias in the correlation functions of its highest and lowest quartiles as well, leading us to expect a merger bias signal, as examined in § 5.

In summary, we confirm and extend previous results to lower redshift and higher mass for concentration-dependent bias. We see a smaller signal for formation time bias, and we see very little (if any) signal for bias based on when halos reach half of their mass. Bias in concentration and half-mass redshift have been seen in previous work for smaller masses at higher redshift; our results show a smaller bias, but well within errors, at least for the concentration-dependent bias.

5. MERGER BIAS

In the previous section we demonstrated the dependence of $\xi(r)$ on halo formation history, characterized by an average property such as the “formation time.” As halo assembly histories are punctuated by large jumps from major mergers, we can also ask whether the clustering of recently merged halos differs from that of the general population.

Although the concept of a major merger is intuitively easy to understand, there is no standard definition in the literature of “merger” or “major merger” (these terms will be used interchangeably henceforth). In simulations, where the progenitors can be tracked and masses measured, major mergers can be defined in terms of masses of the progenitors and the final halo. We define progenitors as those halos at an earlier time that contributed at least half of their mass to a later halo at the time of interest. The three most common ways to define a halo merger are (1) the mass ratio of the two largest progenitors, $M_2/M_1 < 1$; (2) the same ratio, but using the contributing mass of the two most mass-contributing progenitors; and (3) M_f/M_i , the ratio of the current halo mass to the total mass of its largest progenitor at an earlier time. We also consider (4) M_f/M_1 , the ratio of the current halo mass to the largest contributed mass. In our simulations the merger fraction per $0.7 h^{-1}$ Gyr with $M_2/M_1 > 0.3$ increases by more than a factor of 3 from $z = 0$ to 1.

One way to quantify how well the two-body criteria (M_2, M_1 and M_f, M_i) describe the halo growth is to consider the ratio $(M_1 + M_2)/M_f$. This ratio is 1 for a halo formed only from its two largest predecessors: a two-body merger with no other accretion. It is lowered by accretion or multibody mergers. Figure 3 shows the cumulative distribution of $(M_1 + M_2)/M_f$ for halos with $M > 10^{14} h^{-1} M_\odot$ satisfying a variety of merger criteria. We considered both cases where M_1 and M_2 are the full and contributing progenitor masses. As can be seen on the right, for all halos with $M > 10^{14} h^{-1} M_\odot$ at $z = 0$, considering mass gains within the last $0.4 h^{-1}$ Gyr, at least 5% of the final halo mass is not from the two largest contributors. As the merger criteria are hardened (i.e., the merger is more “major”), the two largest progenitors contribute less and less of the final mass. As can be seen on the left,

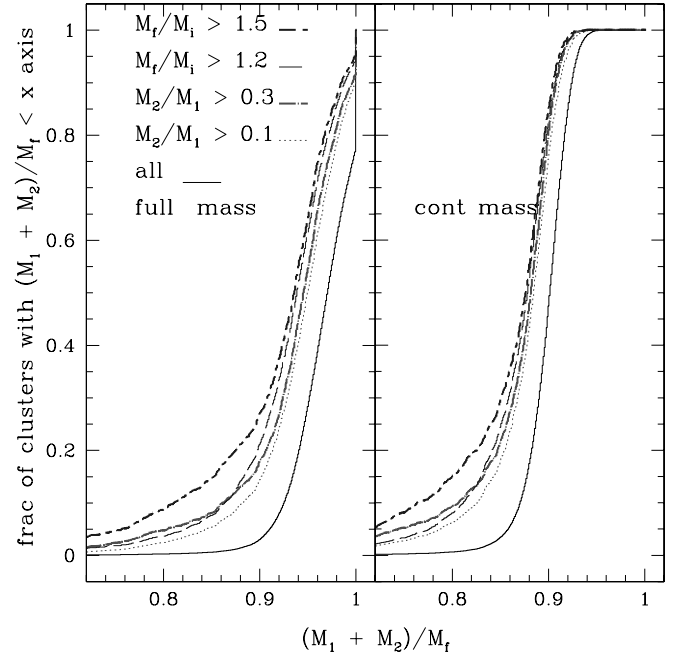


FIG. 3.—Cumulative distribution of $(M_1 + M_2)/M_f$ for different subsamples of our $b = 0.15$ halos at $z = 0$. Looking back $0.4 h^{-1}$ Gyr the subsamples are defined by $M_f/M_i > 1.5$, 1.2 or $M_2/M_1 > 0.3$, 0.1 . The lines are in the same order, top to bottom, with the lowest line being the full sample. At left M_1, M_2 are the full masses of the two largest progenitors; at right M_1, M_2 refer to the contributing mass. [See the electronic edition of the Journal for a color version of this figure.]

the same amount of mass as found in the two largest progenitors makes up the entire mass of the final halo in $\sim 25\%$ of the full sample of halos. Lengthening the time step or looking to higher redshift also increases the fraction of halos getting their mass from halos other than the two largest progenitors. For simplicity, our subsequent analysis uses only the two-body criteria to define mergers, so the accuracy of this assumption as examined above should be kept in mind.

Previous work to identify a merger bias through N -body simulations and analytic methods gives a mixed picture. Gottlöber et al. (2002) found a clustering bias for recently ($\Delta t = 0.5$ Gyr) merged objects with $M_f/M_i > 1.25$ and $M \leq M_*$ at $z = 0$. These authors, however, did not try to match the mass distribution of the comparison sample to that of the merged halos, which is a problem since mergers occur more often for more massive halos and the bias is known to increase with halo mass. To isolate the effects due to merging, the comparison sample needs to have the same mass distribution as the merged sample, and most subsequent work has ensured this. Percival et al. (2003) found no bias between the correlation functions of recently merged ($\Delta t = 10^8$ yr, $M_2/M_1 > 0.3$) and general samples at $z = 2$ for halos with $M \sim M_*, 25M_*$, and $150M_*$. Scannapieco & Thacker (2003) confirmed the Percival et al. (2003) results for major mergers in a $z = 3$ sample for a smaller range of masses but surprisingly found an enhancement of clustering for halos with recent ($\Delta t = 5 \times 10^7, 10^8$ yr) large total mass gain, $M_f/M_i > 1.20$. That is, they find a bias when selecting halos with recent large mass gains, but not when selecting on recently merged halos’ parent masses. Their signal was weak due to limited statistics.

That the previous literature is inconclusive is to be expected, given that the effects of merger history on clustering are small and extremely difficult to measure numerically. We expect the largest signal when $M \gg M_*$, but this is where the number density of objects is smallest. In addition, the most extreme mergers are the

rarest, increasing the shot noise in the measurement of $\xi(r)$. If we include more common events, the “merged” and “comparison” samples become more similar, washing out the signal of interest. At higher redshift, the merger rate increases; thus, the merged and comparison samples have more overlap unless the merger ratio is increased, leading to worse statistics. To try to overcome these statistical effects, we use our very large samples of simulated halos to search for a merger, or temporal, bias.

To define a “recent major merger” requires both a choice of threshold for one of the merger ratios and a choice of time interval. As we expect the halo crossing time to be $\sim 0.7 h^{-1} \text{Gyr}$ (e.g., Tasitsiomi et al. 2004; Gottlöber et al. 2001; Rowley et al. 2004), we expect that outputs at this separation or shorter are small enough to catch recently merged halos while they are still “unrelaxed.” That is, a “recent merger” might be expected to correspond to a dynamically disturbed halo.

We consider the four merger criteria mentioned above, as well as a wide range of samples and merger definitions. We used nine different time intervals from $z \approx 1$ to $z = 0$ as given in § 2. We considered four different thresholds for both M_2/M_1 and M_f/M_i using both total and contributing mass of the progenitors: $M_2/M_1 > 0.1, 0.2, 0.3, 0.5$ and $M_f/M_i > 1.2, 1.3, 1.5, 2.0$. Furthermore, we used two minimum masses, 5×10^{13} and $10^{14} h^{-1} M_\odot$, and two FoF linking lengths, $b = 0.15$ and 0.2 . Combinations of each of these criteria resulted in over 700 different pairs of “merged” and “comparison” samples. Although this data set is very rich, systematic trends are difficult to identify. This is in part because increasing the merger “strength” simultaneously increases the noise (due to lower numbers of events).

Evidence of bias is very slight in the binned $\xi(r)$. We used three methods to try to isolate the signal: the marked correlation function, the integrated correlation function, and a likelihood fit to a power law for the correlation function. The clustering and merger criteria influence these three quantities in distinct ways. We now describe each method and our corresponding results in turn.

5.1. Marked Correlation Function

One problem with computing merger effects in terms of $\xi(r)$ is that, to compute the difference in clustering of merged and random samples, one must define a Boolean merger criterion: a halo is either in the merged sample or not. As halo histories are complex, a more nuanced measure of merger clustering is useful, and this can be provided by using the marked correlation function (Beisbart & Kerscher 2000; Beisbart et al. 2002; Gottlöber et al. 2002; Sheth & Tormen 2004; Harker et al. 2006; Sheth et al. 2005). Each of N objects gets assigned a mark, m_i , for $i = 1, \dots, N$. Denoting the separation of the pair (i, j) by $r_{i,j}$, the marked correlation function, $M(r)$, is defined by

$$M(r) = \sum_{ij} \frac{m_i m_j}{n(r) \bar{m}^2}, \quad (6)$$

where the sum is over all pairs of objects (i, j) with separation $r_{ij} = r$, $n(r)$ is the number of pairs, and the mean mark, \bar{m} , is calculated over all objects in the sample. The marked correlation function “divides” out the clustering of the average sample, and thus a difference in clustering is detected for $M(r) \neq 1$.

We consider five marks: M_2/M_1 (for both total and contributed masses), M_f/M_i , M_f/M_1 (where M_1 is contributed mass), and $\frac{1}{2}(1 + M_2/M_1)$. The last case had a smaller range of marks and thus tests sensitivity to extreme events. The results for this mark were similar to the others, suggesting that we are not dominated by outliers. Halos are chosen with mass in a narrow range, $M_{\min} < M < \sqrt{2}M_{\min}$, to minimize the previously mentioned bias due to

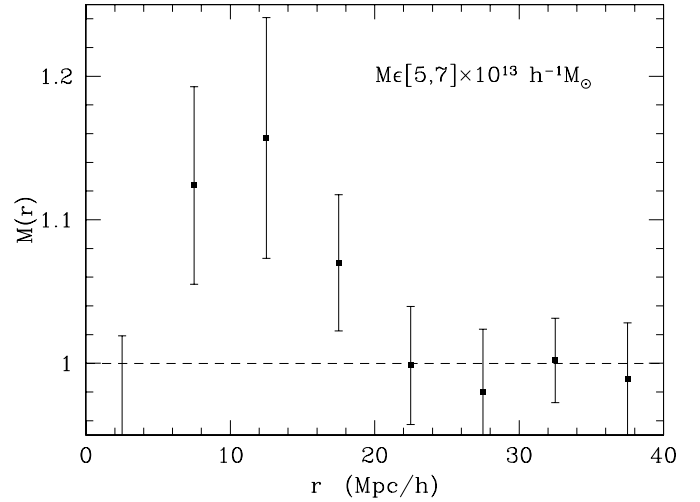


FIG. 4.—Marked correlation function for halos in the range $(5-7) \times 10^{13} h^{-1} M_\odot$ at $z = 0$. The mark is the maximum progenitor mass ratio, M_2/M_1 , within the last $1 h^{-1} \text{Gyr}$. The error bars come from dividing the sample into eight octants.

merged halos being more massive. The global bias changes less than a percent over the mass ranges we consider.

In our combined sample of several output times and mass ranges, the largest signal comes from using as a mark the maximum value of M_2/M_1 within Δt of the present, as shown in Figure 4. As Δt was increased the signal went smoothly to zero. We find similar behavior for $M_2/(M_1 + M_2)$, which suggests that any bias is contributed by the systems where $M_2 \ll M_1$. The signal is extremely weak for the other marks we considered. By stacking the signal across multiple output times (see § 5.3 for details), we are able to find small, but statistically significant, detections of excess power for the marks M_2/M_1 , $M_2/(M_1 + M_2)$, and M_f/M_i , for halos near $5 \times 10^{13} h^{-1} M_\odot$. At higher masses there is weak evidence for an effect, but the large error bars weaken the statistical significance.

As the marked correlation function approach finds only a weak signal, typically an enhanced clustering of order 5%–10%, we also explore two indicators that characterize the correlations by fewer parameters: the integrated correlation function observed at a single scale, and a likelihood fit to a power-law correlation function.

5.2. Integrated Correlation Function

Given an object at some position, the integrated correlation function

$$\bar{\xi}(r) \equiv \frac{3}{r^3} \int_0^r x^2 \xi(x) dx \quad (7)$$

is the probability, above random, that a second object will be within a sphere of radius r . This quantity enhances any increased clustering at short distances but gives error bars that are even more highly correlated than those of the correlation function, $\xi(r)$, itself. A typical result is shown in Figure 5, where a significant signal can be seen. As in the previous section, we find a weak signal regardless of merger definition in our 700 plus samples. Considering all of the samples and all of the separations r , more than $\frac{2}{3}$ of the time the difference $\bar{\xi}_{\text{merge}}(r) - \bar{\xi}_{\text{all}}(r)$ was positive.

This method separates the data into radial bins, requiring us to estimate the clustering at many locations. Since the errors on the binned correlation points are highly correlated, we reduced $\bar{\xi}(r)$ to a single measurement by fixing a preferred scale. The signal

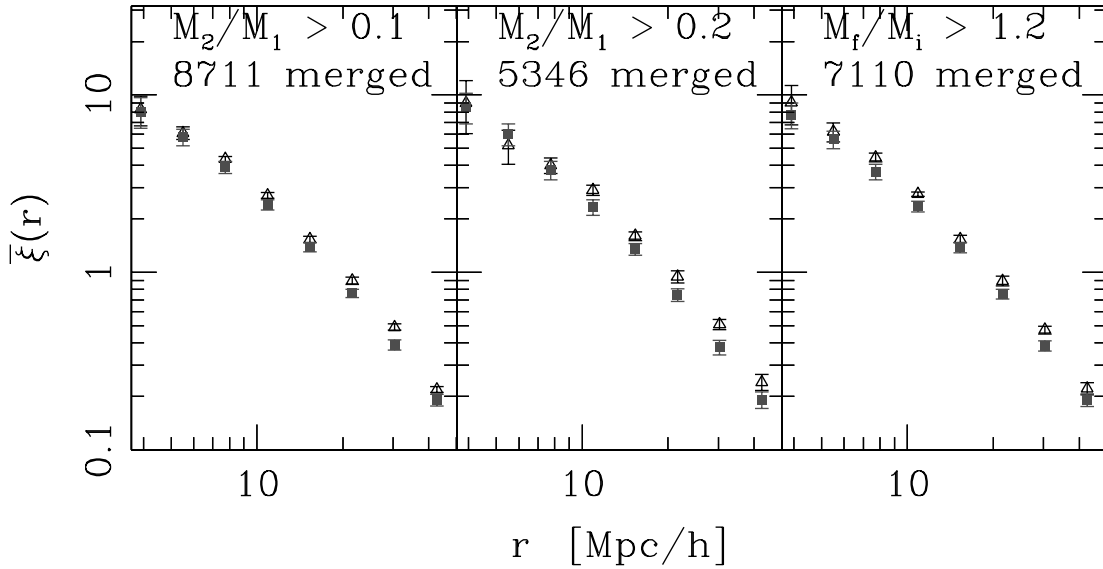


FIG. 5.—Integrated correlation function, $\bar{\xi}(r)$, of recently (within $0.4 h^{-1}$ Gyr) merged halos (triangles) and a comparison sample of the same mass (squares) for $M_2/M_1 > 0.1$ (left), $M_2/M_1 > 0.2$ (middle), and $M_f/M_i > 1.2$ (right), where M_1, M_2 are the full masses of the progenitor halos, for halos in our $b = 0.15$ catalog at $z = 0$. The number of halos that merged out of the 96,319 total halos with $M > 5 \times 10^{13} h^{-1} M_\odot$ is shown at upper right for each case. For these three examples, the differences between the two samples are largest at $30 h^{-1}$ Mpc, with significance 3.1σ (left), 2.7σ (middle), and 2.5σ (right). [See the electronic edition of the Journal for a color version of this figure.]

tends to be largest near $r = 20 h^{-1}$ Mpc (although the signal is largest at $r = 30 h^{-1}$ Mpc in the examples in Fig. 5), and so we compare $\xi(r)$ of the merged and general samples at this radius. On average, when a 2σ signal is seen (5%–15% of the time, depending on mass ratio, etc.), $\bar{\xi}(r)$ for the mergers is $\sim 20\%$ higher than for the general sample, although in extreme cases the difference can be as large as a factor of 2 or 3. Due to the noisy statistics, it was hard to identify any clear trends.

5.3. Likelihood Fit to r_0

The integrated correlation function sums all pairs within a spherical region. As an alternate approach, we approximate the correlation function as a power law over some range of radii,

and we perform a likelihood fit to this power-law correlation function:

$$\xi(r) = \left(\frac{r}{r_0}\right)^{-\gamma} \quad (8)$$

over the range of scales (r_{\min} , r_{\max}). This method incorporates information from many scales, similar to the integrated correlation function. However, it is combined with the expectation that the correlation function should be a power law and excises the center region. By using the positions of the halos directly in the fit to the likelihood, the errors differ from those in the integrated correlation function as well.

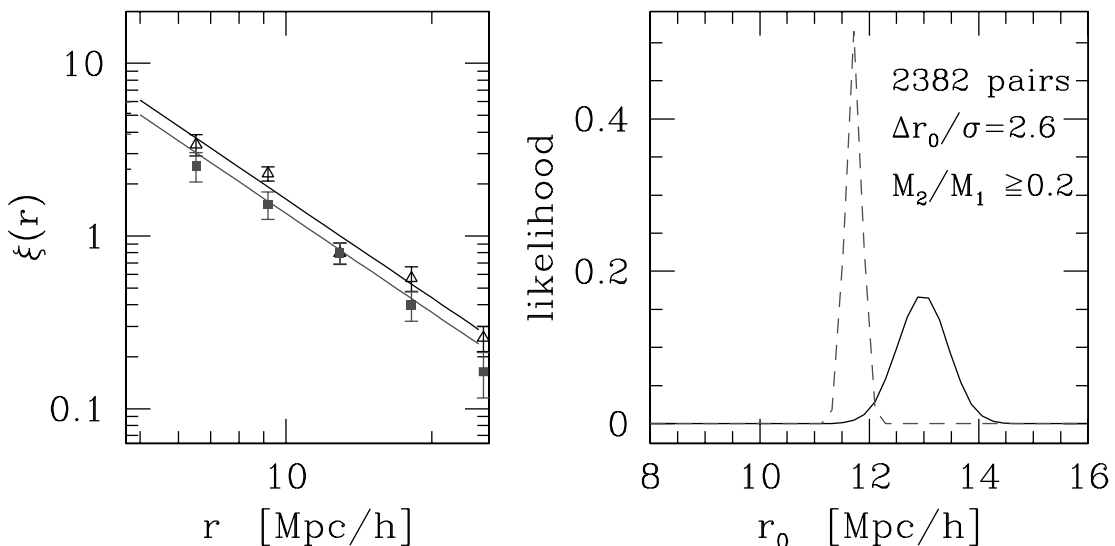


FIG. 6.—Left: Correlation function for a recently merged sample (triangles) and a comparison sample (squares) of the same mass. The lines indicate the best-fit $\gamma = 1.9$ power-law model, fitted directly to the cluster positions [not the binned $\xi(r)$]. Right: Likelihood for the clustering amplitude, r_0 , assuming a slope $\gamma = 1.9$ for the same samples at left. The sample is at $z = 0$, with a minimum mass of $5 \times 10^{13} h^{-1} M_\odot$ ($b = 0.15$), looking back $0.4 h^{-1}$ Gyr. Mergers are tagged as having $M_2/M_1 \geq 0.2$, M_1, M_2 full progenitor masses. [See the electronic edition of the Journal for a color version of this figure.]

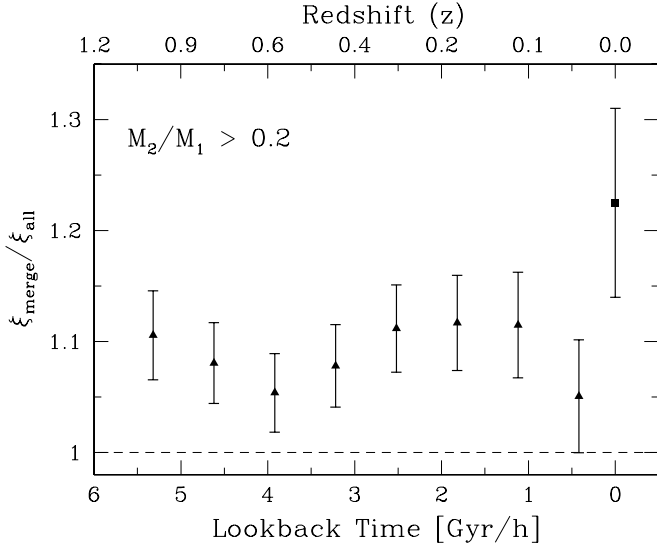


FIG. 7.—Scale-independent ratio of the power-law fit correlation functions for the merged and comparison samples, as a function of look-back time/redshift; $\Delta t = 0.7 h^{-1}$ Gyr (triangles) and $0.4 h^{-1}$ Gyr (square). The mergers satisfy the criterion $M_2/M_1 > 0.2$, with M_2, M_1 total progenitor mass, for the $M > 5 \times 10^{13} h^{-1} M_\odot$ halos in our $b = 0.15$ catalog. No evidence of systematic bias evolution with redshift is found. The enhanced clustering at $z = 0$ arises presumably from the shorter time interval used.

Assuming that the pair counts form a Poisson sample with mean proportional to $1 + \xi(r)$, the likelihood L is (Croft et al. 1997; Stephens et al. 1997)

$$\ln L(r_0) = -2\pi\bar{n}^2 \int_{r_{\min}}^{r_{\max}} r^2 [1 + \xi(r)] dr + \sum_{i<j} \ln(\bar{n}^2 r_{i,j}^2 [1 + \xi(r_{i,j})]) + \text{const}, \quad (9)$$

where the sum is over measured pairs i, j with separation $r_{i,j}$, \bar{n} is the measured average density,¹¹ and $\xi(r)$ is given by equation (8). We fit over the range $5\text{--}25 h^{-1}$ Mpc, where the correlation function exhibits an approximately power-law behavior. For the comparison sample we multiply the likelihoods for several different realizations, to reduce the noise, and then renormalize to unit area. A typical result, where a significant signal can be seen, is shown in Figure 6, demonstrating both the power-law fit and the maximum likelihood distribution. For the fits, r_0 was usually $\sim 10 h^{-1}$ Mpc, within the range where the power-law fit was being applied.

Across all of our samples, we find $\gamma \simeq 1.9 \pm 0.1$. To allow us to compare different samples more easily, we reduce the number of free parameters to one by holding $\gamma \equiv 1.9$. A typical example, demonstrating the ratio of the power-law fit correlation functions of the merged and general sample, is shown in Figure 7 as a function of look-back time/redshift. Since we fix $\gamma = 1.9$ for both the merged and general sample, the ratio $\xi_{\text{merge}}/\xi_{\text{all}}$ using equation (8) is scale invariant within our fit range. While the enhanced clustering of the recently merged sample is small, it remains statistically significant. Typically, the merged sample shows an enhanced clustering of 5%–10% in the correlation function for the $0.7 h^{-1}$ Gyr spacings, although we find no strong evidence of systematic bias evolution with redshift. Moreover, at $z = 0$, where the spacing is smaller ($0.4 h^{-1}$ Gyr), we find a significantly en-

¹¹ We find that marginalizing or maximizing over \bar{n} as a free parameter results in biased fits for several samples.

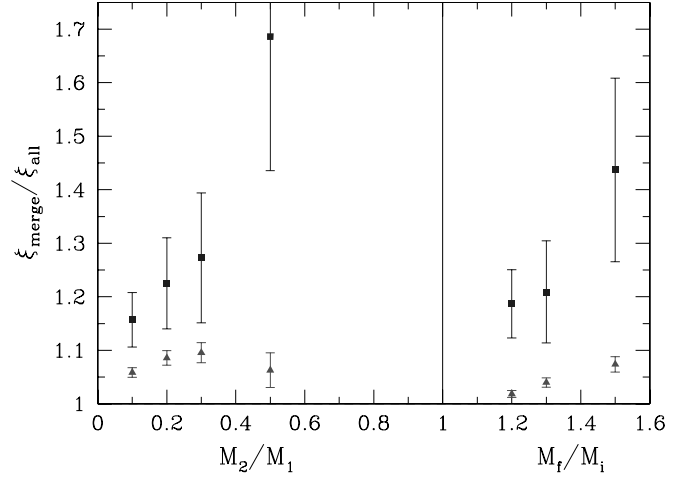


FIG. 8.—Scale-independent ratio of the power-law fit correlation functions for the merged and comparison samples as a function of merger ratio, M_2/M_1 (left symbols; full progenitor mass) and M_f/M_i (right symbols), for halos above $5 \times 10^{13} h^{-1} M_\odot$ in our $b = 0.15$ catalog. Mergers are counted within $0.4 h^{-1}$ Gyr of $z = 0$ (squares), and an average across all $0.7 h^{-1}$ Gyr spacings from $z \approx 1$ to $z = 0.04$ (triangles). In both cases, clear trends can be seen. [See the electronic edition of the Journal for a color version of this figure.]

hanced $\xi(r)$ for the mergers, often 10%–20%. Presumably, this increased clustering signal is caused by the smaller time interval. Larger intervals encompass more mergers, leading to smaller errors, but also leading to a smaller signal, since mergers now encompass a more significant fraction of the comparison population. As mentioned above, looking at earlier times also makes the merged and comparison population overlap increase dramatically.

By averaging $\xi_{\text{merge}}/\xi_{\text{all}}$ across all of the $0.7 h^{-1}$ Gyr spacings from $z \approx 1$ to $z = 0.04$, we are able to study the size of the merger bias simply as a function of merger ratio. Figure 8 shows the increase of $\xi_{\text{merge}}/\xi_{\text{all}}$ with M_2/M_1 (full mass) and M_f/M_i both for mergers within $0.4 h^{-1}$ Gyr of the present and for the redshift-averaged $0.7 h^{-1}$ Gyr spacings. The merger bias clearly increases with increasing merger ratio, with the smaller time step yielding stronger clustering as described above.

In summary, we find a weak bias in many cases (but not all: the signals are very noisy) for recent major mergers and recent large mass gains. While Percival et al. (2003) found no such merger bias, our signal is consistent with their upper limit of 20% on the bias effects of recent mergers. The work of Scannapieco & Thacker (2003) saw a small bias for large mass gains but noted that their statistics limited their ability to determine the significance. Our larger box allowed us to incorporate the effects of cosmic variance, which had been neglected in previous work. Cosmic variance increased the errors by 40% or more, which limited the significance of the signal. Nonetheless, we still found a small bias for *both* mergers and large mass gains.

6. CONCLUSIONS

The large-scale structure of the universe is built on a skeleton of clustered dark matter halos. For the past two decades we have known that rarer, more massive dark matter halos cluster more strongly than their lower mass counterparts. Halos of a fixed mass, however, can differ in their formation history and large-scale environment, and recent work on halos smaller than galaxy clusters has shown that this can lead to further changes in their clustering.

In this paper we have used two large-volume, high-resolution N -body simulations to study the clustering of massive halos as a function of formation history. We confirmed earlier results

that the lower concentration massive halos are more clustered than the population as a whole, extending these results to higher masses (and thus lower redshifts) than had been probed previously (Wechsler et al. 2006). [Previous work had looked at similar regimes of M/M_* but for smaller M and thus higher redshift; note again that exact scaling with M/M_* is not expected for non-power-law $P(k)$ and $\Omega_m \neq 1$.] Similarly, we confirmed the enhanced clustering of halos with later formation times, although the signal was not as strong as for concentration. The signal for bias based on a halo reaching half of its mass is weaker than that seen in Gao et al. (2005) (again for higher z) and not statistically significant in our case.

We also investigated whether recent merger activity affected the clustering of massive halos, a topic with a muddled history in the literature. While we found statistically significant ($>2\sigma$) merger effects on clustering in many cases we considered, both for recent major mergers and large mass gain, in most cases this signal was weak: a 5%–10% increase in bias. Our strongest signal came from using a likelihood fit of the correlation function to a power law, particularly for major mergers within $0.4 h^{-1}$ Gyr of the present, where we saw a typical merger bias of up to 20%. This bias signal is not necessarily at odds with the lack of signal in previous work, which looked for larger bias than that seen on average here.

Even with a $(1.1 h^{-1} \text{ Gpc})^3$ volume, massive halos remain very rare objects and small changes in their correlations are difficult to detect. We were plagued by the competing effects that increasing the severity of the merger (and hence underlying sig-

nal) decreases the number of pairs, worsening the statistics. General trends remain elusive, since changing various criteria (e.g., merger definition, minimum mass, time step) generally changed the number of halos involved, thus changing the errors. However, we did find that the strength of the merger bias typically increased with increasing merger ratio, i.e., more major mergers are more strongly biased. Finally, we note that the correlations found between the last large (20%) mass gain and the different definitions of formation redshifts provide a connection between the assembly bias studied in § 4 and the merger bias in § 5. This bias is not expected from direct application of extended Press-Schechter theory, and it provides a phenomenon that a more precise analytic model of mergers should reproduce.

We thank J. Bullock, R. Croft, G. Jungman, P. Norberg, G. Rockefeller, R. Sheth, E. Scannapieco, R. Wechsler, and A. Zabludoff for enlightening conversations and especially R. Sheth and R. Wechsler, who also provided useful comments on the draft. J. D. C., D. E. H., and M. W. thank the staff of the Aspen Center for Physics for their hospitality while this work was being completed. The simulations and analysis in this paper were carried out on supercomputers at Los Alamos National Laboratory and NERSC. J. D. C. was supported in part by the NSF. M. W. was supported in part by NASA. D. E. H. gratefully acknowledges a Feynman Fellowship from LANL.

REFERENCES

- Beisbart, C., & Kerscher, M. 2000, *ApJ*, 545, 6
- Beisbart, C., Kerscher, M., & Mecke, K. 2002, in *Morphology of Condensed Matter*, ed. K. Mecke & D. Stoyan (Berlin: Springer), 358
- Benson, A. J., Kamionkowski, M., & Hassani, S. H. 2005, *MNRAS*, 357, 847
- Bond, J. R., Cole, S., Efstathiou, G., & Kaiser, N. 1991, *ApJ*, 379, 440
- Bower, R. G. 1991, *MNRAS*, 248, 332
- Bullock, J. S., Kolatt, T. S., Sigad, Y., Somerville, R. S., Kravtsov, A. V., Klypin, A. A., Primack, J. R., & Dekel, A. 2001, *MNRAS*, 321, 559
- Cohn, J. D., & White, M. 2005, *Astropart. Phys.*, 24, 316
- Colberg, J. M., et al. 2000, *MNRAS*, 319, 209
- Cole, S., & Kaiser, N. 1989, *MNRAS*, 237, 1127
- Cooray, A., & Sheth, R. 2002, *Phys. Rep.*, 372, 1
- Croft, R. A. C., Dalton, G. B., Efstathiou, G., Sutherland, W. J., & Maddox, S. J. 1997, *MNRAS*, 291, 305
- Croton, D. J., Gao, L., & White, S. D. M. 2006, *MNRAS*, in press (astro-ph/0605636)
- Davis, M., Efstathiou, G., Frenk, C. S., & White, S. D. M. 1985, *ApJ*, 292, 371
- Efstathiou, G., Frenk, C. S., White, S. D. M., & Davis, M. 1988, *MNRAS*, 235, 715
- Furlanetto, S. R., & Kamionkowski, M. 2006, *MNRAS*, 366, 529
- Gao, L., Springel, V., & White, S. D. M. 2005, *MNRAS*, 363, L66
- Gao, L., White, S. D. M., Jenkins, A., Stoehr, F., & Springel, V. 2004, *MNRAS*, 355, 819
- Gottlöber, S., Kerscher, M., Kravtsov, A. V., Faltenbacher, A., Klypin, A., & Müller, V. 2002, *A&A*, 387, 778
- Gottlöber, S., Klypin, A., & Kravtsov, A. 2001, *ApJ*, 546, 223
- Hamana, T., Yoshida, N., Suto, Y., & Evrard, A. E. 2001, *ApJ*, 561, L143
- Harker, G., Cole, S., Helly, J., Frenk, C., & Jenkins, A. 2006, *MNRAS*, 367, 1039
- Kaiser, N. 1984, *ApJ*, 284, L9
- Kauffmann, G., & Haehnelt, M. 2000, *MNRAS*, 311, 576
- Kitayama, T., & Suto, Y. 1996a, *ApJ*, 469, 480
- . 1996b, *MNRAS*, 280, 638
- Lacey, C. G., & Cole, S. 1993, *MNRAS*, 262, 627
- . 1994, *MNRAS*, 271, 676
- Landy, S. D., & Szalay, A. S. 1993, *ApJ*, 412, 64
- Lemson, G., & Kauffmann, G. 1999, *MNRAS*, 302, 111
- Lupton, R. 1993, *Statistics in Theory and Practice* (Princeton: Princeton Univ. Press)
- Mihos, J., & Hernquist, L. 1996, *ApJ*, 464, 641
- Miller, L., Percival, W. J., Croom, S. M., & Babić, A. 2006, *A&A*, 459, 43
- Mo, H. J., & White, S. D. M. 1996, *MNRAS*, 282, 347
- Navarro, J. F., Frenk, C. S., & White, S. D. M. 1996, *ApJ*, 462, 563
- . 1997, *ApJ*, 490, 493
- Peacock, J. A. 1999, *Cosmological Physics* (Cambridge: Cambridge Univ. Press)
- Percival, W. J., Scott, D., Peacock, J. A., & Dunlop, J. S. 2003, *MNRAS*, 338, L31
- Rowley, D. R., Thomas, P. A., & Kay, S. T. 2004, *MNRAS*, 352, 508
- Sarazin, C. L. 2005, in *X-Ray and Radio Connections*, ed. L. O. Sjouwerman & K. K. Dyer (Socorro: NRAO), <http://www.aoc.nrao.edu/events/xraydio>
- Scannapieco, E., & Thacker, R. J. 2003, *ApJ*, 590, L69
- Seljak, U., & Warren, M. S. 2004, *MNRAS*, 355, 129
- Sheth, R. K., Connolly, A. J., & Skibba, R. 2005, *MNRAS*, submitted (astro-ph/0511773)
- Sheth, R. K., & Pitman, J. 1997, *MNRAS*, 289, 66
- Sheth, R. K., & Tormen, G. 1999, *MNRAS*, 308, 119
- . 2004, *MNRAS*, 350, 1385
- Stephens, A. W., Schneider, D. P., Schmidt, M., Gunn, J. E., & Weinberg, D. H. 1997, *AJ*, 114, 41
- Tasitsiomi, A., Kravtsov, A. V., Gottlöber, S., & Klypin, A. A. 2004, *ApJ*, 607, 125
- Wang, H. Y., Mo, H. J., & Jing, Y. P. 2006, *MNRAS*, in press (astro-ph/0608690)
- Warren, M., & Salmon, J. 1993, in *Supercomputing '93*, 12
- Wechsler, R. H., Bullock, J. S., Primack, J. R., Kravtsov, A. V., & Dekel, A. 2002, *ApJ*, 568, 52
- Wechsler, R. H., Zentner, A. R., Bullock, J. S., Kravtsov, A. V., & Allgood, B. 2006, *ApJ*, 652, 71
- White, M. 2001, *A&A*, 367, 27
- . 2002, *ApJS*, 143, 241
- White, S. D. M. 1996, in *Cosmology and Large-Scale Structure*, ed. R. Schaefer et al. (Dordrecht: Elsevier), 349
- Zhao, D. H., Jing, Y.-P., Mo, H.-J., & Boerner, G. 2003a, *ApJ*, 597, L9
- Zhao, D. H., Mo, H.-J., Jing, Y.-P., & Boerner, G. 2003b, *MNRAS*, 339, 12